Identification and Analysis of Intermetallic Phases in Overaged Zr-containing and Cr-containing Al-Zn-Mg-Cu Alloys

X. M. Li[1*] and M. J. Starink[2]

[1]School of Materials Science and Engineering, Southeast University,
Nanjing 211189, P.R. China

[2]School of Engineering Sciences, University of Southampton,
Southampton SO17 1BJ, UK

*Corresponding author:
Telephone: 86-25-83366459
Fax: 86-25-52090669
Email: xmli6@seu.edu.cn

Abstract

This paper investigates the effect of alloying elements on the characteristics of intermetallic phases in Zr-containing and Cr-containing 7xxx Al-Zn-Mg-Cu alloys at overaged conditions. Four Al-Zn-Mg-Cu alloy plates with different alloying element contents were studied by optical microscopy based image analysis, differential scanning calorimetry, scanning electron microscopy combined with energy disperse X-ray spectroscopy and transmission electron microscopy. The grain structures, recrystallisation, intermetallic phases and precipitates in the selected alloys have been analysed and the presence of coarse intermetallic phases has been interpreted using established phase diagrams. The different effects of Zr or Cr addition to the alloys have been compared. The experimental results showed that the recrystallised area fraction of Zr-containing alloys is less than that of Cr-containing alloys, being attributable to Zr reducing recrystallisation more effectively than Cr. The detected particles are mainly S phase, Al_7Cu_2Fe, as well as dispersoids of Al_3Zr for Zr-containing alloys and Cr-rich E phase for Cr-containing alloys. These coarse particles, especially the S phase which can not be dissolved during solution treatment, are detrimental to the fracture toughness of the alloys.

Keywords: Intermetallic phases; Zr-containing; Cr-containing; Al-Zn-Mg-Cu alloys

1. Introduction

The high strength of Al-Zn-Mg-Cu (7xxx series) alloys is obtained through age hardening process. The main precipitation sequence is generally given as:

Supersaturated Solid Solution $(SSS\alpha) \rightarrow$ GP zones $\rightarrow \eta' \rightarrow \eta$

η is a solid solution of $MgZn_2$ with a hexagonal structure. GP zones are clusters of solute atoms and have an approximately spherical shape. The intermediate precipitate η' may form from GP zones and is thought to have the same structure of η phase although the lattice parameters are different. Other precipitation reaction involves the formation of S (Al_2CuMg) phase, and T ($Mg_3Zn_3Al_2$) phase depending on alloy composition [1-4].

The main properties of 7xxx series alloys are greatly determined by the main phases in the equilibrium state. Thus, a good balance of properties can be obtained by microstructural

modifications via alloy compositional changes and heat treatment variations [5-8]. Available literature indicates that recrystallisation reduces toughness and increases quench sensitivity of the alloys [9-10]. Coarse intermetallic particles (larger than 1μm) are generally detrimental to the properties, especially to the toughness, and in 7xxx alloys these particles are especially the Fe-rich and S phases [11-13]. Consequently, detailed investigation into the microstructure of 7xxx alloys with an aim to optimise the properties is of key interest to materials researchers.

Many advances in the studies of microstructural evolution, grain structures and coarse intermetallic particles of 7xxx series alloys have been reported [2-5, 7, 13]. For instance, Alvarez et al studied the dendrite and intermetallic growth of solidified Al–Zn–Mg alloys and the results of characterization and prediction of microstructure were used to select an appropriate Al–Zn–Mg alloy composition for the applications in corrosive environment [2]. Microstructure and mechanical properties of a spray-deposited Al–Zn–Mg–Cu alloy processed through hot rolling and heat treatment have been investigated by Wang et al. The fragmentation of the $Mg(ZnCu)_2$ phases in the alloy was found during hot rolling and after solution treating, Al_7Cu_2Fe and Al_9FeNi compounds were also identified [5]. In the work of modelling grain boundary strengthening in ultra-fine grained aluminum alloys by Nes et al [7], the mechanical properties of aluminum alloys with fine grain sizes were modelled and well related to their microstructural characteristics. However, The effects of Zr and Cr additions on the microstructural variations of Al-Zn-Mg-Cu alloys have rarely been systematically studied and analyzed.

The objective of this paper is to investigate how compositional variations affect the microstructural features of 7xxx Zr-containing and Cr-containing alloys through a range of analytical techniques. We will specifically study grain structures, recrystalisation, coarse intermetallic particles and precipitates in the four alloys at overaged conditions. The presence of coarse intermetallic particles will be interpreted using phase diagrams and comparison of different effects of Zr and Cr on the microstructural characteristics will be presented.

2. Experimental Procedures

2.1 Materials
The alloys in this study are two Zr-containing aluminium alloys, Al-6.1Zn-2.3Mg-1.9Cu (A1) and Al-6.1Zn-2.3Mg-2.6Cu (A2) as well as two Cr-containing aluminium alloys, Al-5.74Zn-2.17Mg-1.52Cu (B1) and Al-6.16Zn-3.02Mg-1.98Cu (B2) alloys. The compositions of A1 and A2 are within the compositional windows of commercial 7050 alloy, containing 0.08-0.15wt%Zr, and those of B1 and B2 are close to 7075 alloy, containing 0.18-0.28wt%Cr. The alloys were produced at Qinetiq, Farnborough, UK. The alloys were processed using conventional casting procedures, and after stress relaxation and homogenization, the ingots were divided into two halves. Each of the halves was hot worked and the final stage was hot rolling to 25mm thick plates of about 1 meter length and 0.2m width. The alloys were solution treated at temperature 475°C for 1h and quenched and subsequently aged at 172°C for various ageing times. These ageing treatments are typical T7 type overaged conditions.

2.2 Microstructural Examination

2.2.1 Optical Microscopy
Optical Microscopy linked with image analysis software was mainly used to examine the grain structures of the alloys. The optical microscopic equipment used was an Olympus BH2. Image analysis software for Windows developed by Foster Findlay Associates Limited was employed for analysis of grain structure and particles in the samples. The image analysis package is linked to the optical microscope using a high resolution digital camera for image acquisition [14]. Samples were cut at about half plate thickness along the three main planes, i.e. the LT, TS and LS planes. (L = longitudinal rolling direction, T = long transverse and S = short transverse.) Specimens were mounted in Bakelite and ground successively with a final finish of 1200 grit. Subsequent polishing was

performed using 6μm, 1μm and finally ¼ μm diamond paste on cloth wheels under lubricants. For grain structure examination, samples were etched in $10cm^3$ H_3PO_4 plus 90 cm^3 distilled water heated to 50°C for about one minute. Image analysis software for Windows developed by Foster Findlay Associates Limited was employed for analysis of grain structure and particles in the samples. The image analysis package is linked to the optical microscope using a high resolution digital camera for image acquisition [14].

2.2.2 Scanning Electron Microscopy / Energy Dispersive X-Ray Spectroscopy

The samples for optical microscopic examination were also used in Scanning Electron Microscopy / Energy Dispersive X-Ray Spectroscopy (SEM/EDS) investigations. The SEM facility was a Jeol JSM-6400 Analytical Scanning Electron Microscope. In general, backscattered electron mode was used. Different areas on the TS sections were scanned to reveal the existing particles. Chemical compositions of various particles in the samples were measured using EDS. With the available composition information, the specific particles were identified individually.

2.2.3 Transmission Electron Microscopy

The Transmission Electron Microscopy (TEM) samples were prepared by cutting a material into a thin slice (~0.3mm), subsequently punch it to a 0.3mm diameter disc and grind it to thickness around 0.15mm. The samples were electro-polished using a solution of 70% methanol and 30% nitric acid, maintained at a temperature of between −20°C and −30°C [15]. The TEM facility was a JEOL JEM 2000FX transmission electron microscope. An accelerating voltage of 200 kV was used.

2.2.4 Differential Scanning Calorimetry

For Differential Scanning Calorimetry (DSC) testing, we cut samples from the plates which have been aged for various times at a single temperature typical for a T7 temper. The DSC equipment was a heat flux type Shimadzu DSC-50 [3]. For all the experiments, a pure aluminium reference (99.9%) with a mass and shape close to that of the sample was used. Baseline correction was performed employing experiments consisting of a single DSC run using pure Al samples. The heat flow was calibrated by measuring the heat of fusion of In and Zn as well as the heat capacity of pure Al. The temperature is calibrated by taking the deviation ΔT from the reference temperature, compared with the measured melting points of In and Zn. The DSC samples were machined from the 7xxx plates to discs 5mm in diameter and 1mm in height with average mass of about 63 mg. DSC experiments were performed at heating rate 10°C/min. As standard procedure, each experiment contains 3 heating runs, with the latter two runs being used mainly for heat capacity corrections.

3. Results

3.1 Grain Structures

All the alloys have a partially recrystallised grain structure and contain small amounts of constituent particles. The grain displays a pan-cake shape and its size is around 5μm on average. Statistically, the grain size through-thickness in the Cr-containing alloys is generally smaller than that in the Zr-containing alloys and this is in agreement with the findings of Wagner and Shenoy [9]. Three-dimensional grain structures of A2 and B2 are shown in Fig. 1. The three-dimensional grain structure images were artificially constructed and scanned from the two-dimensional grain structures of three planes, i.e. the LT, TS and LS planes, respectively. It is shown that the coarse particles are distributed randomly in the matrix, with the amount varying according to the alloy compositions. The recrystallised area fractions for the four alloys plus a commercial 7075 alloy were calculated from the micrographs and presented in Table 1. The results show that the recrystallisation area fraction of the Cr-containing alloys (above 56% and 68%, respectively) is much higher than that of the Zr-containing alloys (37% and 24%, respectively), and our experimental alloys (either Zr-containing or Cr-containing) have higher recrystallisation area fraction than the commercial 7075 alloy. It is worth noting that recrystallisation reduces toughness and

increases quench sensitivity of the alloys (see Ref. [9]), it should therefore be limited to a low level.

Table 1 Recrystallised area fraction of Zr-containing and Cr-containing alloys (%)

Alloy	LT	LS	TS	Average
Zr-containing				
A1	33	44	32	37
A2	17	27	27	24
Cr-containing				
B1	63	53	53	56
B2	73	67	64	68
7075	9	24	23	19

3.2 Intermetallic Particles

Digital image analysis package was used to study the intermetallic particles in the alloys. Three cross sections (LT, TS and LS) of samples of the alloys were examined. The particles identified from the image were categorised by their colour grade and size. Fig. 2 presents an **optical** image of alloy A1 on a TS section. Using image analysis with grey scale and size thresholds, we can identify three types of particles, i.e. black particle, big grey particle (size threshold $>1\mu m$), and small grey particle (size$<1\mu m$). The area fraction of each type of particle was measured and results are summarised in Table 2. It is shown that for Zr-containing alloys, the high Cu alloy has the highest percentage of coarse particles, which indicates that Cu plays an important role in the formation of coarse particles. For Cr-containing alloys, B2 with high alloying element contents has a higher volume fraction of coarse particles than B1 with low alloying element content. Overall, there are more coarse particles in Zr-containing alloys than that in Cr-containing alloys.

In order to identify the coarse particles in these alloys, samples of the selected alloys were studied using SEM/EDS. Table 3 presents some examples of the chemical compositions of the particles obtained from EDS, with identification of the phases. Note that in all cases the aluminium matrix

contributes to the compositional analysis. The micrographs of Alloy B1 and Alloy B2 are presented in Fig. 3 and Fig. 4.

Table 2 Volume fraction of coarse particles (%)

Alloy	LT	LS	TS	Average
Zr-containing				
A1	2.62	1.29	1.34	1.75
A2	2.82	3.51	1.61	2.65
Cr-containing				
B1	0.67	0.46	0.58	0.57
B2	0.97	1.35	1.15	1.16

The EDS data indicates that, for the alloy A2, the detected particles are mostly S phase (diameter $\sim 3\mu m$, evenly distributed particles) and Al_7Cu_2Fe (typically $\sim 15\mu m$, clustered in bands). For alloy B2, the detected particles are mostly S phase and Al_7Cu_2Fe, either. There exists a kind of complex particle, as shown in Table 3, namely type 3 and type 4, part of it being Ti, Fe containing phase and part of it being Fe, Cu containing phase (with more Fe than Cu, so it could not be Al_7Cu_2Fe phase). This coarse particle can not be clearly identified in terms of the available phase diagrams. The main particles in 7075 are Al_7Cu_2Fe and no S phase was detected. There are further very few Cr containing particles in 7075, and this could be $(Fe,Cr)_3SiAl_{12}$ intermetallic constituent formed during solidification or $Cr_2Mg_3Al_{18}$ dispersoid formed during homogenisation according to the literature (see Refs. [16-17]). As the Mg signal in EDS testing is very weak, it is thus unlikely to be $Cr_2Mg_3Al_{18}$ dispersoid. To summarise the particles of Cr-containing 7xxx alloys, it is clear that Al_7Cu_2Fe is the major intermetallic particle whilst S phase can be eliminated by adjusting Cu, Mg contents and solution treatment temperature according to S phase solvus. It is also observed that the detected particles in B1 are mostly irregularly shaped Al_7Cu_2Fe with various sizes (largest up to $20\mu m$ in length). There is hardly any S phase across the section, although throughout the scan a type of

small circular particle was observed and could be identified as S phase.

3.3 Precipitates

As mentioned before, the precipitation sequence in 7xxx alloys can take three main forms depending on composition and ageing, and the maximum strength is achieved when η′/η precipitation is involved [1-2, 18-19]. In this work, TEM was employed to reveal the fine microstructure features of the alloys. TEM experiments were performed on the selected alloys A2, B2 at different ageing conditions, as shown in Figs 5-7. Fig. 5 and Fig. 6 present TEM micrographs of the Zr-containing alloy A2, showing the precipitates and the sub-grain features, respectively. Fig. 7 shows the main precipitates as well as round coarse S phase in the matrix for the Cr-containing alloy B2.

TEM investigation revealed the fine microstructure features of the alloys: precipitates in the matrix, grain (or sub-grain) boundaries and the precipitate-free zones (PFZ). It is observed that there are coarse η precipitates (about 50 nm in diameter) on the sub-grain boundaries. There are two reasons why the precipitates on the grain boundary are much bigger than that of the matrix. Firstly, the rapid diffusion of solute atoms into the boundary as a result of the formation of PFZs causes the relatively large precipitates. Secondly, in the PFZs the depletion of vacancies to levels below that needed for nucleation sites results in formation of coarse precipitates [20].

The TEM observation results of alloy B2 for coarse S phase is consistent with the SEM micrograph as shown in Fig. 4.

3.4 DSC Heat Effect Peaks

During DSC heating and cooling process the precipitation and dissolution reactions in the sample are reflected by a number of heat effect peaks in the DSC curves. Fig. 8 shows a DSC curve of alloy A2 aged at 172°C for 8 hours. Previous work [12, 18] evidenced that for the present overaged alloys peak A corresponds to the dissolution of η′, B corresponds to the formation of η whilst peak C represents the dissolution of η. Since all alloys are in the overaged condition, formation and dissolution of GP zones and most of the precipitation of η′ have been completed prior to DSC experiments and thus these reactions are not observed. Two further effects, D and E, are thought to be due to the formation and subsequent dissolution of S phase. Peak F is due to the melting of S phase at around 490°C for the alloy with high Cu content, when the complete dissolution of this phase is not possible at the solution temperature of 475°C [11]. The presence of this phase has been confirmed in the SEM/EDS experiments on alloy A2. The second type of intermetallic found was Al_7Cu_2Fe. Melting of this phase is not observed in DSC experiments because the reaction is obscured by melting of the Al matrix phase.

Table 3 EDS compositional analysis of typical particles in Zr-containing and Cr-containing alloys (at.%)

Alloy	Particle	Al	Cu	Mg	Zn	Fe	Ti	Si	Zr	Cr	Identification
Zr-containing											
A2	Type 1	70.83	14.39	13.41	1.31	0.04	-	0.00	0.03	-	S (Al_2CuMg)
	Type 2	79.81	13.35	0.00	0.94	5.90	-	0.00	0.00	-	Al_7Cu_2Fe
Cr-containing											
B2	Type 1	50.10	24.77	22.78	2.31	0.04	0.00	-	-	-	S (Al_2CuMg)
	Type 2	75.54	15.46	0.14	1.41	7.36	0.07	-	-	-	Al_7Cu_2Fe
	Type 3	74.54	2.97	0.52	2.02	9.59	10.36	-	-	-	Unidentified
	Type 4	84.88	3.24	0.54	1.88	9.46	0.00	-	-	-	Unidentified
7075	Type 2	73.53	17.06	0.00	0.90	8.35	-	0.00	-	-	Al_7Cu_2Fe
	Type 5	78.59	1.60	0.00	1.12	12.98	-	3.50	-	2.23	Unidentified

4. Discussion

The microstructural characterisation of overaged samples of Zr-containing and Cr-containing 7xxx aluminium alloys revealed some interesting points. The experimental results indicated that there exist very substantial microstructural variations between Zr-containing and Cr-containing alloys. Based on other researchers' work we can predominantly evaluate the effect of addition of Zr or Cr to 7xxx series alloys [9, 16, 21-22]. Generally, the addition of Zr or Cr improves grain structure and reduces recrystallisation in 7xxx alloys through precipitation of finely distributed dispersoids, i.e. Al_3Zr for Zr-containing alloys and $Cr_2Mg_3Al_{18}$ for Cr-containing alloys (it is also called Cr-rich E phase). As shown in the Table 1, the recrystallised area fraction of Zr-containing alloys is less than that of Cr-containing alloys, being attributable to Zr reducing recrystallisation more effectively than Cr. As recrystallisation has direct influence on yield strength and toughness of 7xxx alloys, by decreasing yield strength and toughness with increasing recrystallisation fraction [23], it is, hence, a major concern for selection of materials for aerospace applications.

SEM/EDS results showed that Cr-containing alloys made no significant difference in formation of coarse intermetallics compared with Zr-containing alloys (see Table 2, Figs 4, 5), and the difference in the amount of intermetallic particles was caused by overall composition variations. Similarly, from the TEM observations it was evidenced that either Zr or Cr had no noticeable effect on the final precipitates of the alloys [21], although theories indicate that Zr affects precipitation kinetics by retarding GP zones and η' formation and slowing down η precipitation [24]. This effect might lead to smaller size of η precipitates in Zr-containing alloys than those in Cr-containing alloys, which was also discerned by Conserva and Fiorini [Ref. 21].

One of the advantages that the Zr-containing alloys have over the Cr-containing alloys is that Zr-containing alloys display a capability of significantly improving quench sensitivity (the term quench sensitivity indicates the reduction in ageing hardening capability induced by low quenching rates) [20, 25]. The reason for the quench sensitivity improvement by Zr is due to η phase nucleating and precipitating heterogeneously on Al_3Zr dispersoids during cooling from solution temperature. The Al_3Zr dispersoids are incoherent with the matrix and only act as nucleation sites for η phase [26].

The influence of Zr and Cr on the strength and toughness of 7xxx alloys largely depended on particular ageing conditions. For instance, some authors found that Zr-containing alloys in the T8 condition exhibited higher strength and toughness than Cr-containing alloys, whilst in the T73 condition, Cr-containing alloys were inherently tougher than Zr-containing alloys [9, 27]. As all the alloys studied were overaged conditions, and in combination with the low volume fraction of coarse intermetallic particles for the Cr-containing alloys, it is expected that the Cr-containing alloys could have a better fracture toughness than the Zr-containing alloys.

To further interpret the results, we will make use of a temperature dependent solvus diagram for S phase, as shown in Fig. 9, as well as phase diagram of quaternary system Al-Cu-Mg-Zn at 460°C, 6wt%Zn adapted from Strawbridge et al [Ref. 28], as shown in Fig. 10. In Fig. 9, the S phase solvi indicate that at a solution treatment temperature of 475°C, alloys A2 and B2 are in the (α+S) field, thus S phase can not be dissolved in these alloys at this temperature. Alloy A1 is practically on the S phase solvus, and given sufficient solution treatment time, S phase would be expected to dissolve. However, some compositional segregation originating from the solidification process could cause S phase to remain present even after long solution treatment times. Fig. 9 also indicates that no S phase is present for alloy B1 after the alloy has been solution treated at 475°C, whilst complete dissolution of S phase is impossible for alloy A2 and alloy B2, thus an incipient melting of S phase may occur at the temperature of around 490°C. This phenomenon was well observed in the DSC experiment on alloy A2 (see Fig. 8). Moreover, in Fig. 10, the alloys studied are in the area of the dashed rectangular, it

can be seen that the alloys either contain S phase or no S phase at all, depending on Cu, Mg contents in the alloys. These interpretations are also in good agreement with the SEM/EDS findings.

SEM/EDS experiments on the Zr-containing or Cr-containing alloys indicated that the conditions for the presence of coarse particles are basically similar for these two groups of alloys. The detected particles are mainly S phase, Al_7Cu_2Fe, as well as Al_3Zr for Zr-containing alloys and Cr-rich E phase for Cr-containing alloys. Previous research [3, 28-29] found that another type of coarse particles, namely T phase, with composition of $Mg_3Zn_3Al_2$, could appear for 7xxx alloys with Mg content higher than 3.2wt%, thus, for alloy B2, it is possible for T phase to be present when the compositional segregation reaches the areas of α +S +T and α +T (see Fig. 10). However, as this type of phase is difficult to identify merely using SEM/EDS experiments compared to the relatively bigger S phase and Al_7Cu_2Fe particles, and some more DSC experiments on alloys with higher Mg content may be required to verify the melting peak of the T phase, we will not discuss it further in this paper.

5. Conclusions

Optical microscopy, digital image analysis, DSC, SEM/EDS and TEM were employed to study grain structure, coarse intermetallic particles and precipitates in Zr-containing and Cr-containing Al-Zn-Mg-Cu alloys. The main conclusions are drawn as follows:

1. For all the alloys investigated, optical microscopy revealed a partially recrystallised grain structure with about 20~40% recrystallised area fraction for the Zr-containing alloys and over 50% for the Cr-containing experimental alloys, and about 20% for the commercial 7075 alloy. Unrecrystallised grains show a pan-cake shape.
2. The recrystallised area fraction of Zr-containing alloys is less than that of Cr-containing alloys, being attributable to Zr reducing recrystallisation more effectively than Cr. As recrystallisation has direct influence on yield strength and toughness of 7xxx alloys, it remains a major concern for selection of materials for aerospace applications.
3. With regard to coarse intermetallic particles in the Zr-containing and Cr-containing alloys, SEM/EDS and image analysis revealed that the high Cu alloy has the highest volume fraction of coarse particles. SEM/EDS experiments also indicated that the detected particles are mainly S phase, Al_7Cu_2Fe, as well as Cr, Fe-rich intermetallic particles. These coarse particles, especially the S phase which can not be dissolved during solution treatment, are detrimental to the fracture toughness of the alloys.

References

[1] D. Dumont, A. Deschamps, Y. Brechet, Acta Mater, 52 (2004) 2529-2540.
[2] O. Alvarez, C. Gonzalez, G. Aramburo, R. Herrera, J. A. Juarez-Islas, Mater Sci Eng A 402 (2005) 320-324.
[3] M. J. Starink, X. M. Li, Metall. Mater. Trans.A 34A (2003) 899-911.
[4] P. Sepehrband, S. Esmaeili, Mater Sci Eng A 487 (2008) 309–315.
[5] F.Wang, B. Xiong, Y. Zhang, H. Liu, Z. Li, Q. Liu, Mater Sci Eng A 518 (2009) 144-149.
[6] M. J. Starink, S. C. Wang, Acta Mater 57 (2009) 2376-2389.
[7] E. Nes, B. Holmedal, E. Evangelista, K. Marthinsen, Mater Sci Eng A, 410–411 (2005) 178–182.
[8] W. Z. Du, Z. M. Sun, B. L. Shao, T. T. Zhou, C. Q. Chen, Mater. Characterization 56 (2006) 121–128.
[9] J. A. Wagner, R. N. Shenoy,, Metall Trans A 22A (1991) 2809-2818.
[10] H. M. Flower, High Performance Materials in Aerospace. Chapman & Hall, UK, 1995.
[11] A. J. Morris, R. F. Robey, P. D. Couch, E. D. L. Rios, Mater Sci Forum 242 (1997)181-186.
[12] X. M. Li, M. J. Starink, Mater Sci Forum 313-317 (2000) 1071-1076.

[13] G. Sha, Y.B. Wang, X.Z. Liao, Z.C. Duan, S.P. Ringer, T.G. Langdon. Mater Sci Eng A 527 (2010) 4742-4749.

[14] J. Boselli, P. D. Pitcher, P. J. Gregson, I. Sinclair, Scripta Mater 38 (1998) 839–844.

[15] P. J. Goodhew, Specimen Preparation for Transmission Electron Microscopy of Materials. Oxford Univ Press, New York,1984.

[16] J. R. Davis. Aluminium and Aluminium Alloy, ASM Speciality Handbook, ASM International, USA, 1994,

[17] M. J. Starink, X. M. Li, Mater Trans A 34 (2003) 899-911.

[18] J. K. Park, A. J. Ardell, Scr Metall 22 (1988) 1115-1119.

[19] R. R. Sawtell, J. T. Staley, Aluminium 59 (1983) 127-133.

[20] I. J. Polmear, Light Alloys-Metallurgy of the Light Metals, St. Edmundsbury Press Ltd, UK, 1996.

[21] M. Conserva, P. Fiorini, Metall Trans 4 (1973) 857-862.

[22] O. Engler, E. Sachot, J. C. Ehrstrom, A. Reeves, R. Shahani, Mater Sci Technol 12 (1996) 717-729.

[23] R. C. Dorward, D. J. Beerntsen, Metall Mater Trans A 26A (1995) 2481-2484.

[24] A. K. Mukhopadhyay, G. J. Shiflet, E. A. Starke Jr, Scripta Metall et Mater 24 (1990) 307-12.

[25] P. J. Gregson, Aluminium Alloys: Physical Metallurgy, Processing and Properties, in High Performance Materials in Aerospace, edited by Flower, H. M., Chapman & Hall, UK,1995.

[26] H. Suzuki, M. Kanno, H. Saitoh, Aluminium 59 (1983) 944-947.

[27] C. Q. Chen, J. F. Knott, Met Sci15 (1981) 357-64.

[28] D. J. Strawbridge, W. Hume-Rothery, A. T. Little, J Inst Metals, 74 91948) 191-225.

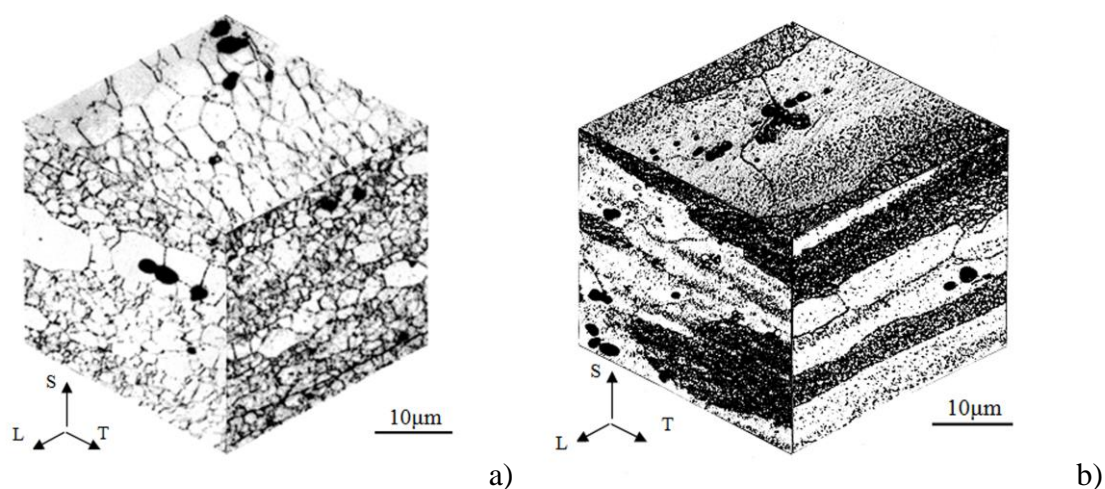[29] J. A. Wert, Scr Metall15 (1981) 445-447.

Fig. 1 a) Three-dimensional grain structures of the Zr-containing Al-6.1Zn-2.3Mg-2.6Cu (wt%) alloy A2; b) Three-dimensional grain structures of the Cr-containing Al-6.16Zn-3.02Mg-1.98Cu (wt%) alloy B2. L = longitudinal rolling direction, T = long transverse and S = short transverse.
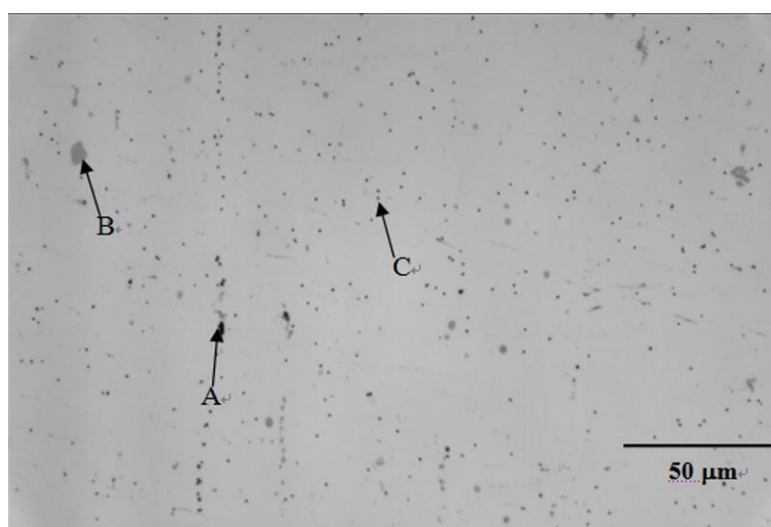

Fig. 2 The optical image of an unetched sample of the Zr-containing Al-6.1Zn-2.3Mg-1.9Cu (wt%) alloy A1 (medium Cu and Mg, TS direction), showing the coarse particles in the matrix. A: black particle, B: big grey particle, C: small grey particle.
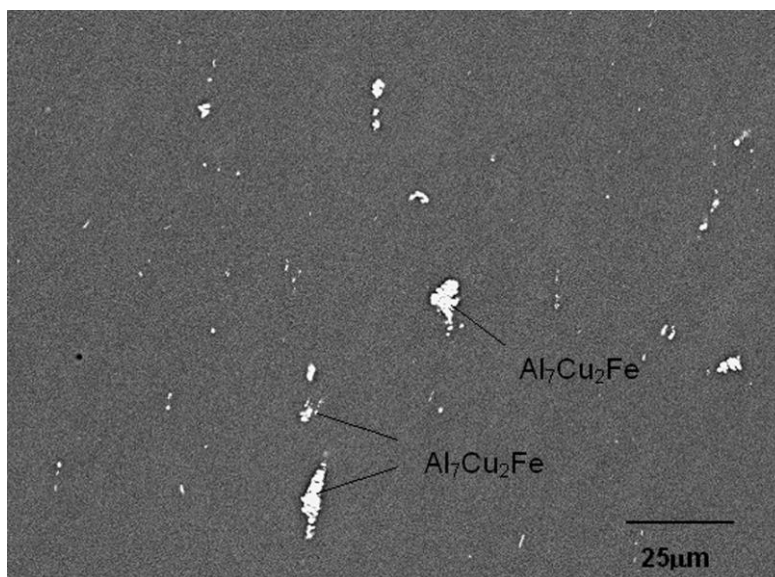
Fig. 3 SEM micrograph of the Cr-containing Al-5.74Zn-2.17Mg-1.52Cu (wt%) alloy B1, showing the main particles: Al_7Cu_2Fe phase.
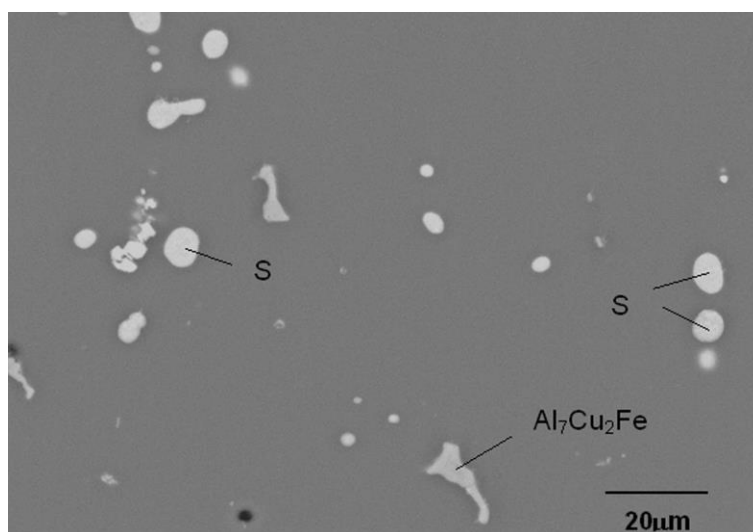
Fig. 4 SEM micrograph of Cr-containing Al-6.16Zn-3.02Mg-1.98Cu (wt%) alloy B2, showing the main particles: S and Al_7Cu_2Fe phases.
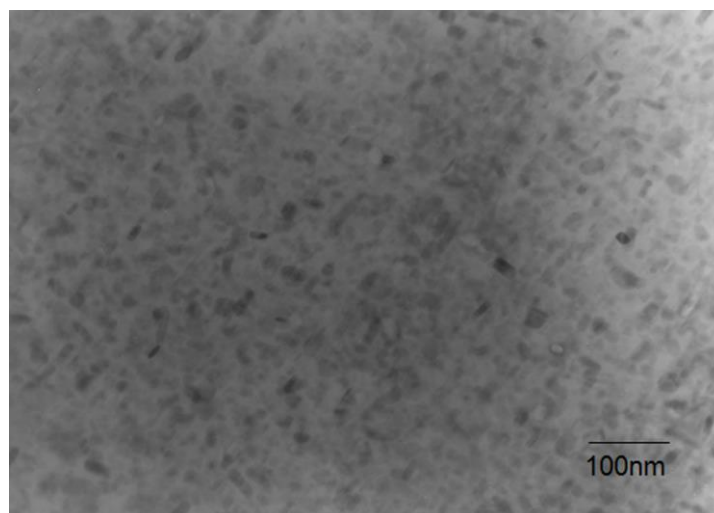
Fig. 5 TEM micrograph of the Zr-containing Al-6.1Zn-2.3Mg-2.6Cu (wt%) alloy A2 aged for 16h at 172°C, showing the main precipitates (bright-field, B=[100]).
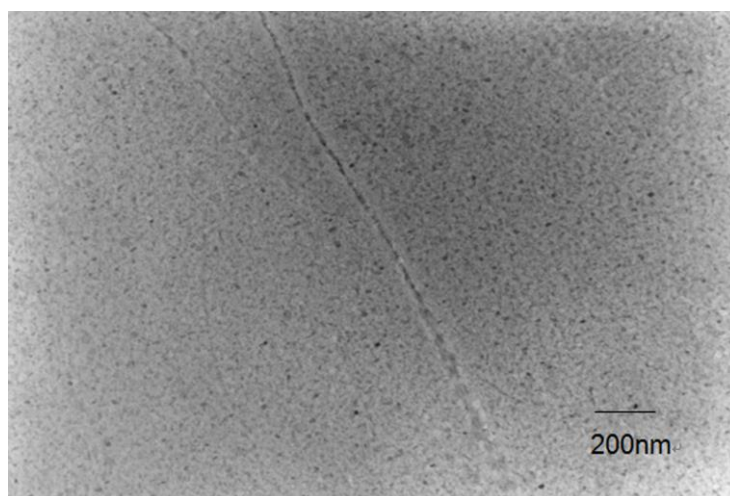

Fig. 6 TEM micrograph of the Zr-containing Al-6.1Zn-2.3Mg-2.6Cu (wt%) alloy A2 aged for 16h at 172°C, showing the sub-grain boundaries (bright-field, B=[100]).
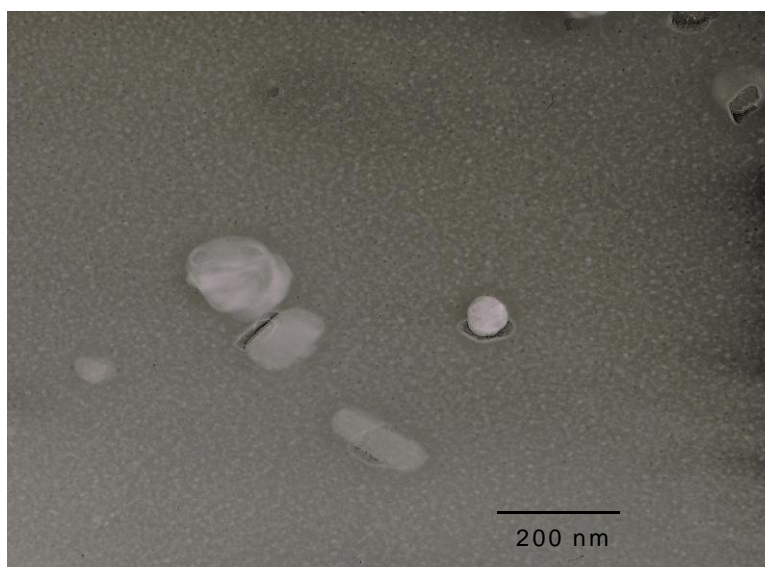
Fig. 7 TEM micrograph of the Cr-containing Al-6.7Zn-2.9Mg-1.9Cu (wt%), alloy B2 aged at 172°C for 4 hours, showing S phase (bright field, orientation is close to [110]).
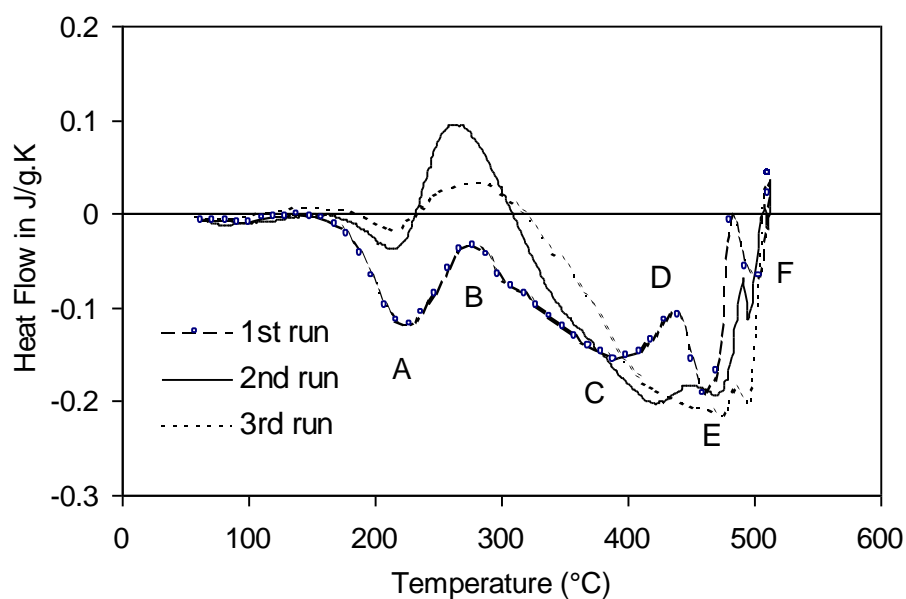

Fig. 8 DSC curves of runs 1 to 3 on Al-6.1Zn-2.3Mg-2.6Cu-0.12Zr (wt%) alloy A2 aged at 172°C for 8 hour, showing dissolution and precipitation of the main phases. Heating rate 10°C/min.
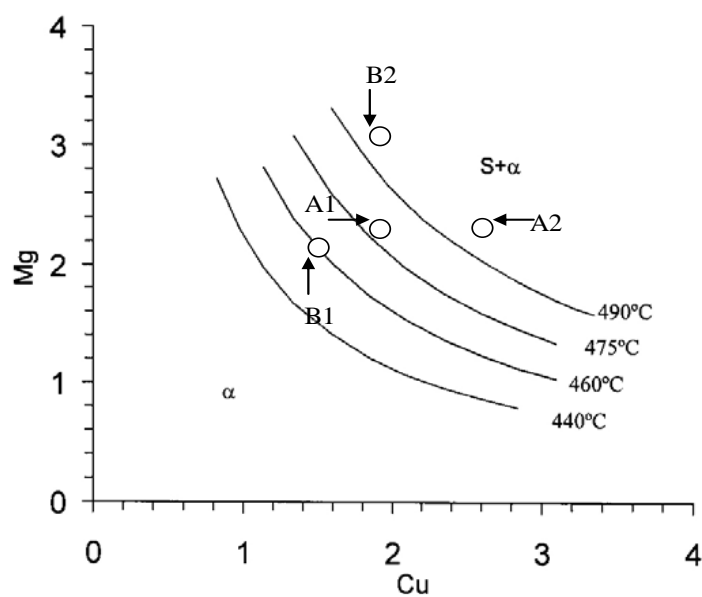
Fig. 9 Solvi of S phase in Al-Zn-Mg-Cu with Zn=6 wt%, temperature range 440-490°C.
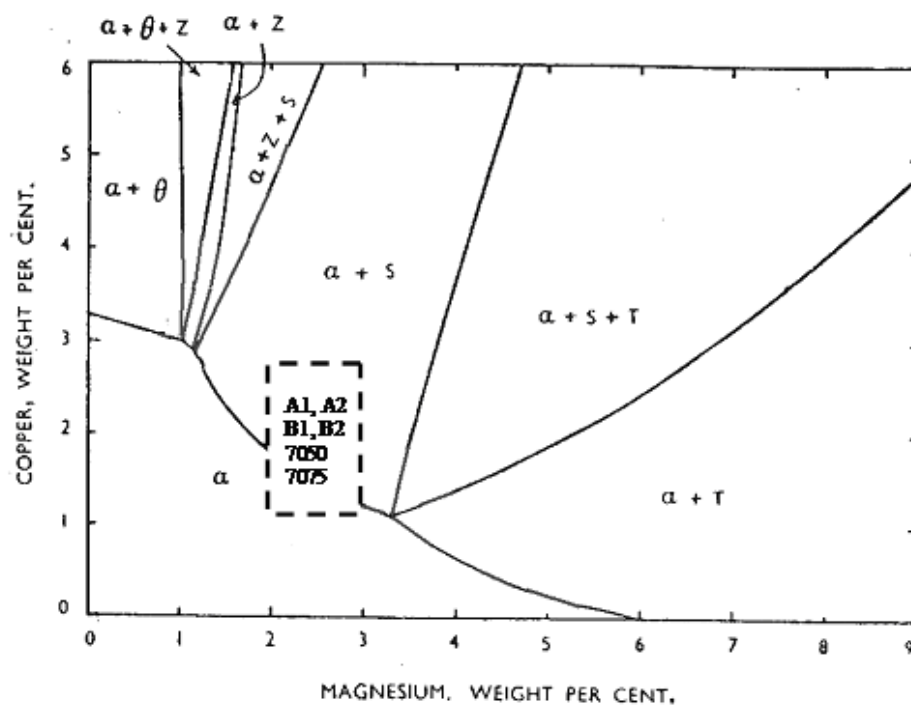

Fig. 10 Quaternary system Al-Cu-Mg-Zn at 460°C, 6%Zn, adapted from Strawbridge et al [Ref. 29].